Vol. 6: 1–19, 1996 | CLIMATE RESEARCH Clim Res | Published January 30

A prognostic phenology scheme for global terrestrial carbon cycle models

Jörg Kaduk*, Martin Heimann

Max Planck Institute for Meteorology, Bundesstr. 55, D-20146 Hamburg, Germany

ABSTRACT: Prognostic and mechanistic schemes for the determination of plant phenological stages from environmental conditions and for the estimation of net primary production (NPP) are presented. The new schemes account for different biomes and are included in a global model of carbon cycling in the terrestrial biosphere. The capability of such a model to simulate the seasonal cycle of atmospheric CO_2 is explored. The model is forced by mean monthly climate variables (temperature, precipitation and light) and the mean annual CO_2 concentration. It predicts atmosphere-biosphere CO_2 exchange fluxes, leaf area index (LAI), and the times of budburst and leaf abcission. The predicted variables can be validated against data on the observed annual cycle of atmospheric CO_2 concentration and against observations of LAI derived from satellite data. The estimated annual NPP of forests appeared realistic; however, the NPP of grass-dominated biomes was greatly underestimated. This seems to be related to the fact that belowground biomass is not explicitly considered in the model. The results of a simulation of the seasonal cycle of atmospheric CO_2 concentration using a 3-dimensional atmospheric transport model were in satisfactory agreement with the observations.

KEY WORDS: Seasonal terrestrial carbon cycle model · Plant phenoloy modelling · Testing terrestrial carbon cycle models · Seasonal cycle of atmospheric CO_2

INTRODUCTION

The terrestrial biosphere represents a major compartment in the global carbon cycle with gross exchange fluxes of 40 to 80 GtC yr^{-1} (1 GtC = 10^{12} kg carbon) (Lieth 1975) which is about 50% of the gross exchange of the atmosphere with all global carbon pools. Terrestrial vegetation alone accounts for ca 99% of the carbon in the living terrestrial biosphere (Whittaker & Likens 1973). Human activities such as de- and afforestation, agricultural practices and burning of wood and fossil fuels interact significantly with the natural carbon cycling in the terrestrial vegetation. Therefore, land vegetation models describing the cycling of carbon through global land vegetation, plant litter, and soil organic carbon (SOC) — the biospheric carbon cycle — can aid in evaluating scenarios for future management of agriculture and forestry, possibly under a climate change scenario as well.

The simulation of consequences of climate change scenarios requires models which are based on plant physiology rather than on correlational methods. Correlations derived from contemporary data relating, for example, net primary productivity to climate (e.g. the MIAMI model; Lieth 1975) are valid only for the present assumed equilibrium state of climate and vegetation. They cannot faithfully describe transient changes of vegetation caused by climate variations. In particular, it is essential to simulate length and timing of the vegetation period on the basis of plant physiological parameters. Reliable estimation of these 2 aspects of the seasonal climate and local vegetation is even more important if biosphere models are to be employed within climate change scenario calculations. For example, although increased summer temperatures might have no direct effect on vegetation development, warming of winter temperatures might lead to a delayed budburst of temperate trees since these require a winter chilling period with temperatures below ca 5°C for rapid budburst in the following spring (Murray et al. 1989).

*E-mail: kaduk@dkrz.de

Researchers have only recently begun to develop mechanistic descriptions of plant phenology that have prognostic power and can be assumed to be valid under a changed climate and different atmospheric CO_2 partial pressures. These are still limited, however, by our incomplete understanding and by the complexity of several plant physiological processes, for example the regulation of growth processes by plants (Wardlaw 1990).

The main objective of the present work was to assess a simulation of the seasonal carbon dynamics of global vegetation, employing a set of climate-dependent, physiologically based rules for phenological sequences. Here we model 2 phenological stages, namely budburst and leaf fall, on the basis of climate-dependent, biome-specific rules, but disregarding direct light effects.

For such an assessment we had to include the phenological scheme in a global biosphere model. Several global biosphere models for the simulation of carbon exchange fluxes have been developed in the past. Their spatial resolutions range from a few boxes representing the global biospheric carbon pools to about $0.5° \times 0.5°$ pixels, e.g. the Terrestrial Ecosystem Model, TEM (Raich et al. 1991), and the High Resolution Biosphere Model, HRBM (Esser 1991, Esser et al. 1994). These modelling approaches employ relations derived from regression analyses (HRBM), remote sensing data (e.g. Heimann & Keeling 1989, Knorr & Heimann 1995), and plant physiological relations (TEM, and the Frankfurt Biosphere Model, FBM; Janecek et al. 1989, Lüdeke et al. 1995).

The structure of our global model is based on the HRBM since it provides a more appropriate structure of biospheric carbon (2 pools of 'living' and 3 pools of 'dead' carbon) for the study of the biospheric carbon cycle than the FBM (2 pools of 'living' and 1 pool of 'dead' carbon) or TEM (1 pool each). Two pools of 'living' carbon (woody, herbaceous) are a minimal structural prerequisite for a realistic modelling of the effects of climate and CO_2 on carbon partioning in the living biosphere. Several carbon pools are needed to describe the different turnover times of the various components in the 'dead' organic carbon.

To estimate annual net primary productivity (NPP), the HRBM essentially relies on the correlational MIAMI model, which relates annual NPP to mean annual temperature and annual precipitation (Lieth 1975); the seasonal distribution of annual NPP and litter production (i.e. the determination of phenology and seasonal NPP) is determined on the basis of satellite data. These approaches cast some doubt on the suitability of the HRBM for prognostic model simulations.

We therefore designed 2 submodules which replace the correlational approach of estimating NPP and the satellite-data-based scheme for defining the temporal distribution of annual NPP and litter production with mechanistic, physiologically based formulations.

Our general approach to determine NPP is based on the scheme applied in the gap model FORSKA (Prentice et al. 1993) for the simulation of patch-scale forest dynamics. It predicts NPP for each plant in a patch, with an annual time step. The environmental effects (temperature, moisture deficit and CO_2) are incorporated as annually averaged scalar multipliers calculated on a daily basis. Nutrient limitations are neglected. However, there are some major modifications in the explicit formulation of our NPP module as compared to FORSKA. In particular, unlike FORSKA, our model determines NPP on a quasi-daily basis from gross primary productivity (GPP) and plant respiration, which are modelled separately. Furthermore FORSKA does not predict phenology on a seasonal basis, as does our model. In addition, in our model there is a coupling between NPP and phenology over the time course of the year which has no parallel in FORSKA. Finally, as an important simplification, in our model NPP is not simulated on a per plant basis but rather on a grid element basis, assuming a homogeneous canopy within each grid element.

The NPP simulation requires that radiation and actual as well as potential evapotranspiration (AET and PET respectively) be specified. Therefore we retained the main parts of the radiation and hydrology simulation schemes from FORSKA. These are based on a simple soil-water bucket model, neglecting vertical structure and vegetation-hydrology interactions.

We consider potential natural vegetation only, assuming a distribution of potential vegetation classified into 17 biomes specified by the BIOME I model by Prentice et al. (1992).

Thus, the complete model described here is based on the BIOME I vegetation map and consists of the radiation and soil-water bucket models from FORSKA, the 2 newly developed mechanistic modules, and the scheme for heterotrophic respiration (litter decay) from the HRBM. Hereafter, 'new model' denotes this specific setup of modules.

The simulation of NPP is based on a mechanistic understanding of plant physiology. Although phenology is derived using a correlational approach, we believe that the resulting formulation reflects specific physiological relations and may be called mechanistic as well. We assume that it is valid, independent of the climate and satellite data used for its derivation. Heterotrophic respiration relies on correlations with temperature and precipitation, as derived by Esser et al. (1982). The water balance model is not mechanistic, in that it does not include a mechanistic approach for the simulation of plant water-uptake.

The newly developed NPP module includes an assimilate pool which represents the starch stored within plants for respiration and budburst in the next growing season (Waring & Schlesinger 1985). This pool is included for a more realistic simulation of respirational processes and the storage of reserves in plants, particularly during the dormant season. Its inclusion allows the following 2 processes to be addressed: (1) Effects of changes in the growing season. For example, a prolonged summer drought might lead to a negative annual balance of GPP and plant respiration, and hence negative annual NPP. The HRBM, in contrast, would always predict non-negative annual NPP. (2) Modifications in plant development due to the amount of assimilates remaining from the previous growing season. Since plant shooting at the beginning of a growing season can only occur if sufficient assimilates remained from the previous growing season, this introduces a dependence of vegetative development in the current growing season on the production conditions in previous years. There is no such connection with previous seasons in the HRBM, where NPP is directly determined from the climate of the current year. Yet both processes might be important during transient climate variations, when vegetation is subjected to conditions to which it is only poorly adapted. The HRBM would always predict the NPP of a vegetation well adapted to the prevailing climate.

The soil-water module is included because the growing potential of vegetation is determined by the seasonal characteristics of soil moisture and not so much by annual precipitation, as assumed in the HRBM. An appropriate simulation of the seasonal time course of soil moisture is even more important for climate change scenarios, since not necessarily its annual mean but its temporal distribution might change (Mitchell et al. 1990). The ratio of AET to PET, as determined from the soil-water module, is used to simulate the effect of drought on assimilation.

In the next section ('Model characteristics') we describe the components of the new model. In the 'Results and discussion' we present the results of an equilibrium run of the new model and discuss these. Since NPP determines the carbon input into the biosphere it must be realistically simulated, and we discuss at some length the power of our model to predict NPP. In a first attempt to validate the new biosphere model, we focus on a simulation of the annual cycle of atmospheric CO_2 concentration. Monthly net biospheric CO_2 fluxes were determined from the biosphere model. These were transferred into the atmospheric transport model TM2 (Heimann & Keeling 1989, Heimann 1995). We then compare the resulting temporal evolution of atmospheric CO_2 concentration with observed seasonal cycles of measured atmospheric CO_2 concentration.

MODEL CHARACTERISTICS

The framework of the global prognostic model for land vegetation presented here is based on the HRBM of Esser (1991), which has a spatial resolution of 0.5° and a time resolution of 1 mo. Within each model grid pixel, the HRBM includes 6 carbon pools — agricultural, natural herbaceous and woody living biomass, herbaceous and woody plant litter, and SOC. To estimate annual NPP, the model relies on the correlational approach of the MIAMI model. In the HRBM, annual NPP is further influenced by empirical soil factors and the atmospheric CO_2 concentration. Litter production rates are derived from an empirical relation between NPP and biomass using the steady state assumption that the annual litter production equals annual NPP. The seasonal distribution of NPP and litter production is estimated from satellite measurements of the Normalized Difference Vegetation Index (NDVI). Litter and SOC decay rates are derived from direct measurements (Esser et al. 1982). The NPP model and, in part, the litter production scheme of the HRBM are replaced in our new model by 2 new modules described below.

Our approach for determining NPP partly follows that used in FORSKA (Prentice et al. 1993). The biome distribution assumed in the new model is that resulting from the BIOME I model by Prentice et al. (1992). The chosen biomes and their phenological type in the new model are given in Table 1. Deciduous biomes are those in which all herbaceous biomass is shed once a year in a short period of time. In evergreen biomes the production rate for herbaceous litter is constant throughout the year. Mixed biomes are assumed to consist of 50% deciduous and 50% evergreen plant types. The 17th biome of Prentice et al. (1992) is called Ice/Polar desert, where we assume no flora, and thus it does not appear in the table.

Since we are not focusing here on climate or CO_2 variations, we do not make any specific distinctions concerning the major photosynthetic pathways (C_3, C_4 and CAM).

In addition to the forcing data of the HRBM (monthly mean temperature, monthly precipitation, mean annual atmospheric CO_2 concentration), the new model requires as input the monthly mean fraction of daylight hours with full sunlight.

In addition to the prognostic variables of the HRBM, the new model predicts carbon storage in the assimilate pool and the time of budburst and leaf abcission. Furthermore, the simple radiation and soil modules simulate the hydrological variables soil water, runoff and AET and PET prognostically. Since we consider potential natural vegetation only, the new model does not predict agricultural biomass as does the HRBM.

Table 1. Biomes considered in the model, their type, and the triggering factors used to initiate budburst and leaf abcission

Biome No.	Biome	Type	Growth trigger	Leaf-fall trigger
1	Tropical Dry Forest/Savannah	Deciduous	NPP	AET/PET
2	Tropical Seasonal Forest	Mixed	NPP	AET/PET
3	Tropical Rain Forest	Evergreen	NPP	AET/PET
4	Xerophytic Woods/Shrub	Evergreen	NPP	AET/PET
5	Hot Desert	Evergreen	NPP	AET/PET
6	Warm Grass/Shrub	Mixed	NPP	AET/PET
7	Broad-leaf Evergr./Mixed Forest	Evergreen	GDD	Temperature
8	Temperate Deciduous Forest	Deciduous	GDD	Temperature
9	Cool Mixed Forest	Mixed	GDD	Temperature
10	Cold Mixed Forest	Mixed	GDD	Temperature
11	Cool Coniferous Forest	Evergreen	GDD	Temperature
12	Cool Grass/Shrub	Mixed	NPP	Temperature
13	Cold Deciduous Forest	Deciduous	GDD	Temperature
14	Boreal Forest	Evergreen	GDD	Temperature
15	Tundra	Mixed	NPP	Temperature
16	Semidesert	Evergreen	GDD	Temperature

The structure of the part of the new model which describes living vegetation is depicted in Fig. 1. In each grid cell there are 3 pools of living biomass [assimilate, herbaceous biomass (leaves and fine roots) and woody biomass (stem, branches and coarse roots)]. GPP, the input into the assimilate pool, is calculated from temperature, the AET/PET ratio, CO_2, and light. Plant respiration, being temperature dependent, depletes the assimilate pool. Vegetation state and the climate variables determine the allocation of the assimilates to herbaceous and woody biomass.

There are also 3 pools of vegetation debris in each grid cell: herbaceous and woody litter and SOC. Litter and SOC production rates depend on vegetation type and the climate variables. Litter and SOC decay rates are determined from the climate variables only.

Thus, in total, the new model consists of 6 carbon state variables (assimilate, herbaceous and woody 'living carbon', herbaceous and woody litter and SOC).

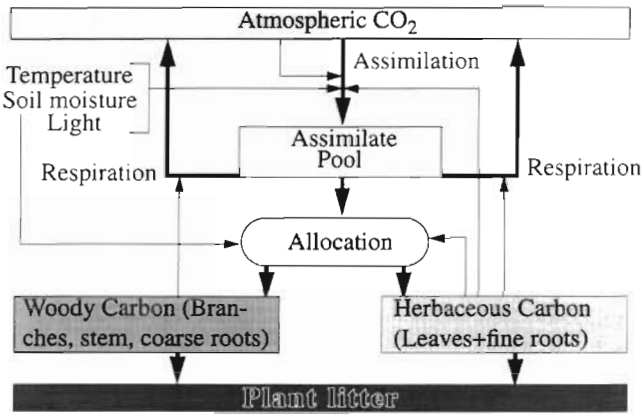

Fig. 1. Structure of the part of the new model of the biospheric carbon cycle which describes living vegetation for each grid cell

Formally, the carbon part of the model is a linear, inhomogeneous system consisting of 6 ordinary first-order differential equations (DE's). The coefficients of the DE's are fixed for each time step. The inhomogeneity results from the NPP calculated as described in the section below on 'The NPP module'. The coefficients of the DE's are defined in the sections below on 'Phenology' and 'Decomposition'.

In principle the radiation and soil water simulations follow the description in Prentice et al. (1993). We mention the most important points briefly.

Radiation

Instantaneous downward short-wave radiation is modelled according to Linacre (1968) as:

$$R_{s,nd}(t) = (c_1 + d_1 S_{nd})(1-\beta) Q_0 \cos(\zeta_{nd}(t_\pi)) \quad (1)$$

where c_1 and d_1 are empirical constants ($c_1 = 0.25$, $d_1 = 0.5$), S_{nd} is the fraction of full sunlight during daylight hours, nd is the day of the year ($nd = 1, \ldots, 360$, i.e. the year is simulated with 360 days), β is the short-wave albedo, and t_π is the time of day. Q_0 and $\cos(\zeta_{nd}(t_\pi))$ are given by:

$$Q_0 = Q_{00}\left[1 + 0.0335\cos\left(\frac{nd}{360}2\pi\right)\right] \quad (2)$$

$$\cos(\zeta_{nd}(t_\pi)) = \sin(lat)\sin(\delta) + \cos(lat)\cos(\delta)\cos(t_\pi) \quad (3)$$

where Q_{00} is the solar constant (1360 W m^{-2}), lat the latitude, and

$$\delta_{nd} = \frac{-23.4^\circ}{360^\circ} 2\pi \cdot \cos\left(\frac{nd+10}{360}2\pi\right) \quad (4)$$

The time of day, t_π, is measured in angular units from solar noon.

The outgoing long-wave radiation, R_l, is estimated according to Linacre (1968) as:

$$R_{l,nd}(t) = (b_1 + (1 - b_1)S_{nd})(a_1 - T_{nd}) \quad (5)$$

where a_1 and b_1 are again empirical constants (a_1 = 107, b_1 = 0.2) and T_{nd} is the mean daily temperature in °C. The diurnal cycle of temperature is neglected. Thus $R_{l,nd}$ is constant during the day.

Net radiation, $R_{n,nd}(t)$, is defined as the difference between $R_{s,nd}(t)$ and $R_{l,nd}$. Daily net radiation results from an integration of $R_{n,nd}(t)$ from sunrise to sunset.

Photosynthetically active radiation (PAR) is assumed to be the frequency band of 400 to 700 nm. Approximately 50% of the short-wave radiation falls into this band. The mean photon density of this frequency band is ~4.6 µE J^{-1} (Landsberg 1986). Thus downward, non-reflected PAR at time t at the top of the canopy, given in µE m^{-2} s^{-1}, is:

$$I_{0,nd}(t) = \frac{0.5}{e^\bullet} R_{s,nd}(t) \quad (6)$$

($e^\bullet$ = 0.22 MJ E^{-1}). Extinction of PAR in the canopy is simulated according to the Beer-Lambert law (Monsi & Saeki 1953):

$$I_{nd}(z,t) = I_{nd}(H_{nd},t) \cdot e^{-k s_{L,nd}(z)(H_{nd}-z)} \quad (7)$$

where z is height above ground, H_{nd} the stand height, k the light extinction coefficient, and $s_{L,nd}(z)$ the leaf density at height z (see Fig. 2). Thus, $I_{nd}(H_{nd},t) \equiv I_{0,nd}(t)$ and plant-absorbed PAR at height z and time t, $I_{ab,nd}(z,t)$, results from:

$$I_{ab,nd}(z,t) = \frac{dI}{dz}(z,t) = k s_{L,nd}(z) I_{0,nd}(t) \cdot e^{-k s_{L,nd}(H_{nd}-z)} \quad (8)$$

H_{nd} depends on the amount of living woody biomass on day nd (see 'Plant respiration' in the section 'The NPP module'). For the sake of simplicity the leaves are assumed to be evenly distributed throughout the canopy and $s_{L,nd}(z)$ is assumed to be constant with height, i.e. $s_{L,nd}(z) \equiv s_{L,nd}$. $s_{L,nd}$ results from the 'reduced' specific leaf area $SLA^\bullet$ (taking belowground biomass into account; see Table 2 and Appendix 1) and herbaceous biomass, ph_{nd}, on day nd:

$$s_{L,nd} = \frac{LAI_{nd}}{H_{nd} - B_{nd}} = \frac{SLA^\bullet ph_{nd}}{H_{nd} - B_{nd}} \quad (9)$$

where LAI_{nd} is leaf area index (m^2 m^{-2}) and B_{nd} bole height on day nd. (Note that LAI is thus linearly related to the model state variable ph.)

Hereafter we drop the argument nd in all model quantities. For a complete list of the model quantities refer to Appendix 1.

The soil water model

From soil water, soil water capacity and daily net radiation (see previous section) we estimate AET and PET as in Prentice et al. (1993), following an approach of Jarvis & MacNaughton (1986). PET is linearly related to net radiation. AET is the minimum of PET and a linear function of actual soil water.

Jarvis & MacNaughton (1986) argue that if soil moisture is not limiting, large-scale evapotranspiration is determined mainly by the energy supply. Thus, for simplicity, we do not consider roots in detail but only the maximal plant-available soil water and fixed matric potentials for the field capacity and the wilting point, which are necessary parameters for the bucket model.

We derived a global spatial distribution of maximal plant-available soil water (soil water capacity between field capacity and wilting point) from the soil texture and depth data of Webb et al. (1992). This was achieved by applying regressions relating soil texture to soil hydraulic properties (from Cosby et al. 1984) assuming a root depth of 1 m if the depth data did not indicate shallower soil. Furthermore we applied globally uniform fixed potentials of 100 hPa for the field capacity and 4500 hPa for the permanent wilting point. These values seem appropriate for general applications (Lerch 1991, Prentice et al. 1992).

The NPP module

For the NPP module we have retained the general approach used in FORSKA (Prentice et al. 1993). However, we simulate gross primary production (GPP) and plant respiration (R) separately. Furthermore we employ the Arrhenius relationship for the temperature dependence of plant respiration instead of a Q_{10} formulation. The canopy is assumed to be homogeneous in the grid element. GPP and R are calculated by an integration through the vegetation canopy, in which photosynthesis and respiration rates are shade-adapted. Unlike FORSKA, our model determines NPP at each time step (6 d in the present model layout), which is important for our new phenology and allocation schemes.

During drought or in the dormant seasons, NPP (= GPP – R) may become negative. All carbon necessary for growth processes is supplied from the assimilate pool. This setup allows for a strong, dynamic response of plants to good growing conditions, as the assimilates can be used for rapid growth.

The basic time step for the NPP submodule is 1 d. The idealized plant structure used in the model is depicted in Fig. 2.

Table 2. Model parameters for the different biomes used; for units see Appendix 1. The values for *SLA*, *rs*, *la*, *lw* and *fh* are from Esser et. al (1994) and Mack (1994)

Biome no.	Biome	A_{max}	T_{min}	T_{max}	T_{opt}	ρ	β	*k*	*fh*	*SLA*	*rs*	*la*	*lw*	ϵ	*a*	*b*	*c*
1	Tropical Dry Forest/ Savannah	15	5	45	21	5977	0.18	0.5	0.90	0.025	0.56	1.0	5	4.0	–	–	–
2	Tropical Seasonal Forest	12	0	50	20	5957	0.15	0.4	0.44	0.024	0.10	1.0	150	3.3	–	–	–
3	Tropical Rain Forest	10	5	50	25	6058	0.13	0.4	0.37	0.025	0.10	1.2	200	3.0	–	–	–
4	Xerophytic Woods/Shrub	10	0	50	30	6160	0.16	0.5	0.40	0.035	0.54	1.0	20	3.3	–	–	–
5	Hot Desert	20	5	60	32	6201	0.20	0.5	0.85	0.028	0.96	1.0	5	4.0	–	–	–
6	Warm Grass/Shrub	18	0	50	30	6160	0.16	0.5	0.90	0.035	0.69	1.0	5	4.0	–	–	–
7	Broadleaf Evergreen/ Mixed Forest	11	2	43	21	5977	0.14	0.5	0.29	0.018	0.20	1.2	130	3.3	34.5	1647	0.150
8	Temperate Deciduous Forest	13	−1	40	20	5957	0.13	0.5	0.38	0.036	0.15	1.0	150	4.0	111.2	1885	0.022
9	Cool Mixed Forest	9	−3	40	15	5855	0.13	0.5	0.38	0.030	0.20	1.0	100	3.5	−14.6	5639	0.025
10	Cold Mixed Forest	10	−5	35	10	5754	0.14	0.5	0.60	0.029	1.27	1.0	60	4.0	−190.0	9993	0.020
11	Cool Conifer Forest	10	−5	35	15	5855	0.13	0.6	0.34	0.011	0.20	2.0	100	2.5	−111.6	9673	0.024
12	Cool Grass/Shrub	9	−3	40	15	5855	0.16	0.5	0.85	0.035	2.03	1.0	10	4.0	–	–	–
13	Cold Deciduous Forest	10	−3	40	10	5754	0.13	0.5	0.38	0.029	1.04	1.0	100	3.5	−190.0	9993	0.020
14	Boreal Forest	10	−3	40	15	5855	0.13	0.5	0.34	0.011	0.23	2.0	100	4.0	−190.0	9993	0.020
15	Tundra	7	−5	40	8	5713	0.15	0.5	0.70	0.030	0.82	1.0	10	4.0	–	–	–
16	Semidesert	5	−5	30	10	5754	0.16	0.5	0.85	0.030	1.44	1.0	15	4.0	−94.0	738	0.010

Instantaneous light-dependent GPP (assimilation), $A(z,t)$, and maintenance respiration, $Rt(z)$, of leaves and wood are determined for each height z in the canopy and at every time t of the day assuming a reference climate condition. These instantaneous rates are integrated through the canopy and over the day to give standard daily rates, GPP_{std} and R_{std} respectively, which are then finally multiplied by factors representing the actual prevailing climate.

GPP_{std} is multiplied by 2 factors, $\Phi_T \equiv \Phi_T(T)$, and $\Phi_D \equiv \Phi_D(AET,PET)$, representing the negative influences of non-optimal temperature and limiting soil moisture, respectively, on photosynthesis. Φ_T and Φ_D vary between 0 and 1. R_{std} is modified by a temperature-dependent respiration factor, $\mu_T \equiv \mu_T(T)$.

Thus daily NPP, NPP_d, is given by:

$$NPP_d = \Phi_T \Phi_D \cdot GPP_{std} - \mu_T \; R_{std} \qquad (10)$$

The influence of the atmospheric CO_2 concentration (CO_2) on photosynthesis is simulated by a growth factor, $\Phi_C \equiv \Phi_C(CO_2)$, modifying the maximal assimilation rate. This influence is accounted for in the formulation of $A(z,t)$.

The explicit equations are given in the following subsections.

Gross primary production. Light-dependent instantaneous gross photosynthesis of the leaf layer at height z in the canopy, $A(z,t)$ is calculated from the

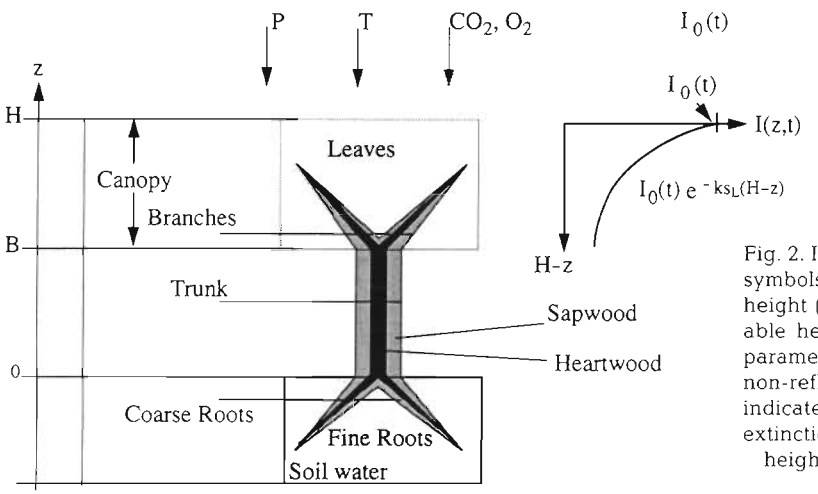

Fig. 2. Idealized plant structure used in the model. The symbols designate: the model variables mean stand height (H), bole height (B), and the independent variable height above ground (z); and the daily forcing parameters precipitation (P), temperature (T), and non-reflected PAR at time t of the day [$I_0(t)$]. The graph indicates light attenuation in the canopy with the light extinction coefficient (k), leaf density (s_L), and PAR at height z in the canopy and time t of the day [$I(z,t)$]

asymptotic function of absorbed PAR:

$$A(z,t) = \frac{\Phi_C s_L P_{max}(z) \phi I_{ab}(z,t)}{\phi I_{ab}(z,t) + \Phi_C s_L P_{max}(z)} \quad (11)$$

where $P_{max}(z)$ is the maximal assimilation rate per square meter at height z in the canopy at 320 ppmv CO_2 (ppmv = parts per million volume) and ϕ is the quantum yield efficiency (Landsberg 1986).

Shade-adapted leaves have lower maximal photosynthetic rates than sun-adapted leaves (Lerch 1991). Therefore the maximal photosynthetic rate of the leaf layer at height z, $P_{max}(z)$, is assumed to equal the rate of the sun-adapted leaves reduced by the fraction of light the layer receives:

$$P_{max}(z) = P_{max}(H) \cdot \frac{I(z,t)}{I_0(t)} = P_{max}(H) \cdot e^{-k s_L (H-z)} \quad (12)$$

For notational purposes we set $A_{max} = P_{max}(H)$, which is the maximal assimilation rate of sun-adapted leaves at 320 ppmv CO_2 in µmol CO_2 m^{-2} s^{-1}.

Substituting Eqs. (8) and (12) into Eq. (11) gives:

$$A(z,t) = k s_L \; e^{-k s_L (H-z)} \frac{\phi I_0(t) \Phi_C A_{max}}{\phi k I_0(t) + \Phi_C A_{max}} \quad (13)$$

hence time and canopy integrations become independent.

Integration of $A(z,t)$ through the canopy and over the day results by using Eq. (9) yields daily light-dependent gross photosynthesis, GPP_{std}:

$$GPP_{std} = (1 - e^{-k\,LAI}) \int_{Day} \frac{\Phi_C A_{max} \phi I_0(t)}{\phi k I_0(t) + \Phi_C A_{max}} \, dt \quad (14)$$

Plant respiration. First the model estimates instantaneous herbaceous tissue and wood maintenance respiration separately at a reference temperature, T_{ref}.

The herbaceous tissue respiration rate at height z and time t in the canopy at the reference temperature, $Rh(z)$, includes the respiration rate of the leaf layer at height z and the respiration rate of those roots supporting these leaves. Since shaded leaves contain less nitrogen and transpire less than sun-exposed leaves, we assume that the respiration rate declines from the top to the bottom of the canopy, like the assimilation rate.

At each height in the canopy the reference respiration rate for herbaceous tissue is assumed to be one tenth of the maximal assimilation rate at optimal temperature.

This assumption is reasonably in line with published measurements (Medina & Klinge 1983, Larcher 1984, Ryan 1993, Sprugel et al. 1995). Further, a combination of reported data relating the maximal assimilation rates and respiration rates with leaf nitrogen content (Evans 1989, Ryan 1991) results in:

$$Rh(H) \approx 0.05 A_{max} \quad (15)$$

As Ryan (1991) mentions, the data used in relating leaf nitrogen content and leaf respiration rates tend to underestimate the respiration. Thus our assumption that $Rh(z) \approx 0.1 P_{max}(z)$ seems reasonable, as it also includes the respiration of the fine roots supporting the leaf layer at height z.

The respiration of wood should not be estimated on the basis of total woody biomass or wood surface area because there may be a large fraction of dead cells in woody plant parts (Ryan 1989). The center of a large stem or branch consists of heartwood which contains no living cells and provides only structural support. On the other hand, the cambium, the phloem, and the sapwood located between the cambium and heartwood contain a certain fraction of living cells. The sapwood is generally able to conduct water and serves to store water and carbohydrates (Waring & Schlesinger 1985), thus it can be considered the life support system for the leaves. In larger stems the main fraction of living cells is located in the sapwood (Ryan 1989). Therefore it seems appropriate to calculate sapwood respiration.

The sapwood volume index, SVI, is defined similarly to LAI and is estimated as:

$$SVI = \int_{-1}^{H} SAI(z)\,dz = \epsilon \int_{-1}^{H} L(z)\,dz$$
$$= \epsilon \left(\int_{-1}^{B} LAI\,dz + \int_{B}^{H} \frac{LAI}{H-B} \cdot z\,dz \right) \approx \epsilon LAI \; H \quad (16)$$

where ϵ is the ratio of accumulated leaf area above height z, $L(z)$, to sapwood cross sectional area at height z in the canopy, $SAI(z)$. Following the pipe model theory, ϵ can be assumed to be a constant (Shinozaki et al. 1964, Waring & Schlesinger 1985).

H is calculated from diameter at breast height, dbh, which in turn is determined from the model state variable woody biomass, pw:

$$dbh = 0.001 pw^{0.521} \quad (17)$$

$$H = 20 dbh^{0.4} \quad (18)$$

The parameters of these allometric relations are derived from data collected by Whittaker & Marks (1975) and from an approximation of an equation used by Prentice et al. (1993).

From the above assumptions on the respiration rate of herbaceous tissue, it follows that:

$$Rh(z) = Rh(H) e^{-k s_L (H-z)} \quad (19)$$

For total respiration at height z at the reference temperature we obtain:

$$Rt(z) = Rh(H) e^{-k s_L (H-z)} + Rs \cdot SAI(z) \quad (20)$$

where Rs is the sapwood respiration rate at temperature $T = T_{ref}$, in µmol CO_2 m^{-3} s^{-1}

Integration of respiration through the canopy and over the day (neglecting the diurnal temperature cycle), and substituting Eq. (16) for the integrated sapwood area index ($S^H SAI(z)\,dz$) yields the standard daily respiration rate, R_{std} (µmol m^{-2} d^{-1}):

$$R_{std} = 86400\left(\frac{Rh_{max}}{k s_L}\left(1-e^{-k\,LAI}\right)+Rs\,\epsilon\,H\cdot LAI\right) \quad (21)$$

$Rh_{max} = 0.1A_{max}$ is the maximal respiration rate of herbaceous biomass (sun-exposed leaves and their fine roots) at temperature = T_{ref}, in µmol CO_2 m^{-2} s^{-1}; Rs is assumed to be $100 \cdot Rl_{max}$.

Environmental factors. We will also refer to the environmental factors Φ_T, Φ_D, Φ_C and μ_T as indices as they are in fact indicators of the vigour of assimilation and respiration in the respective temperature, moisture and CO_2 regimes.

The temperature index, Φ_T, is defined as:

$$\Phi_T(T) = \begin{cases} 1.5\dfrac{(T-T_{min})^{1.5}(T_{max}-T)}{(0.6(T_{max}-T_{min}))^{2.5}} & T_{min} \le T \le T_{max} \\ 0 & \text{otherwise} \end{cases} \quad (22)$$

using mean daily temperature, T. Φ_T is a root function, being 0 at T_{min} and T_{max} and 1 at $T_{opt} = \frac{2}{5}(T_{min}+1.5T_{max})$. This is an empirical fit to the temperature dependence of the activity of the enzymes which first accept CO_2 during metabolism (Johnson et al. 1954, Lommen et al. 1971). Using such an empirical function has the advantage that only 2 reasonably well-known parameters, T_{min} and T_{max} (see e.g. Larcher 1984), have to be specified. The essential drawback is that the optimal temperature range calculated by Eq. (22) is quite small.

The drought index, Φ_D, is modelled by the ratio of actual to potential evapotranspiration,

$$\Phi_D = \frac{AET}{PET} \quad (23)$$

Actual and potential evapotranspiration are calculated using the soil water model (discussed above).

Φ_C, the functional dependence of $A(z,t)$ on the atmospheric CO_2 concentration, is simulated as in Prentice et al. (1993):

$$\Phi_C = 1+\frac{0.7(CO_2-320)}{0.7\cdot 320-\Gamma} \quad (24)$$

where CO_2 is the mean annual atmospheric CO_2 concentration of the current year and Γ is the CO_2 compensation point of photosynthesis, both expressed in ppmv.

Standard daily respiration is modified by the Arrhenius relationship, $\mu_T(T)$:

$$\mu_T(T) = e^{-\rho\left(\frac{1}{T^K}-\frac{1}{T_{ref}^K}\right)} \quad (25)$$

T^K is the mean daily temperature and T_{ref}^K is the reference temperature, T_{ref}, in Kelvin. ρ is chosen such that a Q_{10} of 2 results at 20°C (Amthor 1984, Sprugel et al. 1995).

Phenology

Budburst and leaf abcission are initiated in response to environmental variables. Note that leaf fall implies the shedding of fine roots due to the structure of the model, which assumes a fixed root/shoot ratio.

For both budburst and leaf fall, the biomes were divided into 2 categories according to triggering factors (Table 1).

Leaf growth initiation. Budburst in the tundra, the tropical biomes, and the grasslands is assumed to be NPP-regulated. The vegetation grows whenever growth conditions are favourable, indicated by calculated values of $\frac{dNPP}{dLAI}$ larger than 0. All other biomes are temperature-regulated in the model. They require a certain amount of 5°C-based growing-degree-days, GDD_5. This amount depends on the number of days with mean daily temperature below 5°C, NCD_5 (Murray et al. 1989). Budburst is triggered as soon as the following condition is met:

$$GDD_5 \ge a+be^{-c\,NCD_5}. \quad (26)$$

The rationale for this relation is that the more cold days have passed in the time course of winter and spring, the smaller the chance that new leaves might be damaged by a sudden frost, and thus the lower the GDD_5 requirement may become.

The parameters a, b, and c were derived from a separate evaluation of NDVI data for each biome. We used the mean of the NDVI data for each biweekly interval from 1986 to 1991 (Gallo 1992).

For this derivation the vegetation distribution of the BIOME I model could not be used because it does not include agricultural areas and hence does not show the existing biome distribution. Therefore a comparison with satellite data which refer to the actual vegetation would introduce a misfit. Instead, we used the vegetation distribution given by Olson et al. (1983), as their data are explicitly based on an assessment of actual existing vegetation. Olson et al. (1983) employ vegetation types different from the BIOME I biomes of Prentice et al. (1992), but most of these types can be assigned to one of the BIOME I biomes (Table 3).

Using this assignment we classified most *existing natural* vegetation according to Olson et al. (1983) into the BIOME I biomes; thus, only those pixels entered the evaluation of the NDVI data which were actually occupied by the biome considered, assuming that the Olson et al. (1983) data match the real vege-

Table 3. Ecosystem complexes distinguished by Olson et al. (1983) (with ecosystem numbers in parentheses) and their assignment to the BIOME I biomes according to Prentice et al. (1992). Coastal edges, wetlands [heaths, moors (24); marsh, swamp (35); mangroves (36); bogs, bog woods (38)] and agricultural areas [cool crops (11); warm crops (12); paddylands (14); cool field/woods (28); warm field/woods (29); warm forest/field (30); cool forest/field (31)] have been excluded

Biome no.	Olson et al. (1983) ecosystem complex	Biome I types
1	Tropical savannah (27), tropical dry forest (13)	Tropical Dry Forest/Savannah
2	Tropical seasonal forest (9)	Tropical Seasonal Forest
3	Equatorial evergreen forest (10)	Tropical Rain Forest
4	Highland shrub (20), Mediterranean grazing (21), semiarid woods (22), succulent thorns (25), low shrub (37)	Xerophytic Woods/Shrub
5	Warm irrigated dryland (15), hot desert (39), sand desert (43)	Hot Desert
6	Warm grass/shrub (19)	Warm Grass/Shrub
7	Warm mixed forest (6), warm conifer forest (7), tropical montane complexes (8)	Broad-leaf Evergreen/Mixed forest
8	Warm deciduous forest (5)	Temperate Deciduous Forest
9	Cool mixed forest (4)	Cool Mixed Forest
11	Cool conifer forest (3)	Cool Coniferous Forest
12	Cool irrigated dryland (16), cool grass/shrub (18), Siberian parks (23)	Cool Grass/Shrub
14	Main taiga (2), northern taiga (26), southern taiga (32), equatorial southern taiga (33)	Boreal Forest
15	Cold irrigated dryland (17), wooded tundra (41), tundra (42)	Tundra
16	Cool desert (40)	Semidesert
17	Polar desert (44), ice (45)	Ice

tation distribution during the time period of the NDVI data.

For each pixel within the biome areas of the reclassified Olson et al. ecosystem types, we interpreted the date of the largest increase in the NDVI data after the monthly mean temperature had reached 5°C as an indication of budburst. From the climate data we determined GDD_5 and NCD_5 up until those dates. For each biome we obtained a set of GDD_5 and NCD_5 data pairs representing the climate conditions up to the time of budburst. Eq. (26) was fitted to these data pairs for each biome.

It remains somewhat questionable whether the data of Olson et al. (1983) really represent the vegetation distribution detected by satellites. Clearly this is very uncertain, considering the fact that there is a more than 10 yr difference between collection of the data used by Olson et al. (1983) and the NDVI data. However, it seems reasonable to assume that the mismatch is relatively small in the temperate biomes. Furthermore, because of the continuity of all mathematical operations involved in the derivation of the coefficients for Eq. (26), the error in these coefficients introduced by small misfits in the vegetation distribution is expected to be small as well.

Unfortunately Olson et al. (1983) do not distinguish between the biomes Boreal Forest, Cold Mixed Forest and Cold Deciduous Forest, and therefore no parameters could be derived for the last 2 biomes. Instead, we used the parameters obtained for Boreal Forest. This presumably is not appropriate — at least not for the Cold Deciduous Forest — as we show below.

Allocation. Allocation depends on the environmental conditions prevailing during the current time step. Formally it is defined by 2 coefficients, h_2 and h_3, which are calculated every time step and which determine the fractions of the assimilate pool that are transferred to herbaceous and woody living biomass, respectively.

The extent of leaf area is of crucial importance for plants. A large LAI is advantageous as it allows more photosynthesis (gross production). On the other hand, it requires higher investments of material and energy in maintenance and construction, which eventually reduce the net carbon gain.

Accordingly, the value of the currently optimal LAI, which is still physically possible, is central in the model allocation scheme. This LAI value, LAI_{max}, is defined as the smaller of 2 indicators of the current climate and model state: firstly, the optimal LAI, giving rise to maximal NPP under the prevailing growing conditions, LAI_{npp}; and secondly, the maximal LAI which could be maintained physically by the vegetation, LAI_{veg}, i.e. the LAI value which is structurally the maximum possible with the current amount of biomass. Thus, LAI_{max} =

$\min(LAI_{npp}, LAI_{veg})$, where LAI_{npp} is determined from $\frac{dNPP}{dLAI}(LAI_{npp})$ assuming the prevailing growth conditions. LAI_{veg} is derived from the reduced specific leaf area, SLA^*, and a fixed fraction of total plant biomass, fh, relating total plant biomass, p_{tot}, to herbaceous plant biomass:

$$LAI_{veg} = SLA^* \cdot fh \cdot p_{tot}. \quad (27)$$

As soon as budburst is triggered, h_2 and h_3 are defined by the following equations:

$$h_2 = \frac{LAI_{max} - LAI}{LAI_{max}} \cdot \min\left(0.25, \frac{pa}{3pl_{max}}\right) \quad (28)$$

$$h_3 = \min\left[\frac{pa}{3pl_{max}}\left(1 - \frac{LAI_{max} - LAI}{LAI_{max}}\right), \frac{pw_{max}}{pa}\right] \quad (29)$$

where pa is the size of the assimilate pool, pl_{max} the amount of herbaceous phytomass corresponding to LAI_{max}, and pw_{max} the maximal amount of woody biomass (defined as a fixed fraction of total plant biomass, $pw_{max} = fw \cdot p_{tot}$). The term $\frac{pa}{3pl_{max}}$ ensures that growth is slowed down as soon as the amount of carbon in the assimilate pool drops below 3 times the currently optimal amount of herbaceous biomass. If necessary, the values of h_2 and h_3 are adjusted such that $0 \le h_2, h_3 \le 1$. The fractions relating total plant biomass to woody and herbaceous plant biomass, fh and fw, are the same as those used in the HRBM (see Table 2) (Mack 1994, Esser et al. 1994).

Litter production. Litter production is proportional to the corresponding pool sizes. In evergreen biomes herbaceous litter production occurs at a fixed rate throughout the year. In the case of deciduous types, leaf fall in the tropical biomes is assumed to be regulated by soil moisture, and in the temperate biomes to be triggered by temperature. Tropical biomes initiate leaf fall whenever $AET/PET \le 0.4$; temperate biomes initiate leaf fall when the mean monthly temperature drops below 5°C. The production rate for woody litter is constant throughout the year in each biome. Both these rates are derived from the turnover times of herbaceous and woody tissue as defined in the HRBM. For the sake of simplicity, leaf area of mixed biomes is assumed to be 50% deciduous and 50% evergreen. For deciduous types we assume that leaf fall occurs over the course of 1 full month. Thus, in mixed biomes the leaf litter production rates are adjusted such that, 1 mo after the start of leaf fall, $(\frac{1}{2} * \frac{1}{12 \times 2})$ of the initial herbaceous biomass is shed, assuming that the turnover time of the evergreen herbaceous material is 2 yr. 11% of the herbaceous and 30% of the woody litter produced are transferred to the SOC pool (Esser 1991), the remainder to the corresponding litter pools.

Decomposition

The daily decomposition rates of herbaceous and woody litter as well as SOC are defined by the relations obtained by Esser et al. (1982) and Esser (1991) from measurements adjusted by the time step length:

$$ldr_x = \frac{\log 2}{360 \times 50} \cdot \min(ldT_x, ldp_x); \quad x = \text{h or w} \quad (30)$$

$$ldT_h = 7.67 \cdot \exp(0.0926(T_t + 6.41)) + 17.06 \quad (31)$$

$$ldp_h = \left(\frac{50}{0.0215 + \exp(4.2 - 0.0053p_t)} + 670\right) \times \left(\frac{0.094}{0.7 + \exp(-0.0023p_t - 5.05)} + 0.076\right) \times 0.64(1 - \exp(-0.001p_t)) \quad (32)$$

$$ldT_w = 2.67 \cdot \exp(0.0522(T_t + 31.63)) - 2.51 \quad (33)$$

$$ldp_w = \left(\frac{27.8}{0.021 + \exp(8.53 - 0.0095p_t)} + 712\right) \times \left(\frac{0.126}{1.51 + \exp(-0.003p_t - 4.65)} + 0.05\right) \times 0.5(1 - \exp(-0.001p_t)) \quad (34)$$

$$ldr_s = 0.01\, ldr_h \quad (35)$$

where T_t is the mean temperature of the time step, p_t is the precipitation of the time step multiplied by 360/(timestep length in days) and h, w, and s refer to herbaceous and woody litter and SOC.

RESULTS AND DISCUSSION

The model was run with daily calculation of NPP and an integration time step of 6 d. The daily climate data were generated by a linear interpolation of climatological mean monthly data from the database of the International Institute for Applied Systems Analysis (IIASA) (Leemans & Cramer 1991). The atmospheric CO_2 concentration was kept constant at 338 ppmv. After 300 yr of simulation the model calculated a global annual NPP of about 47 GtC yr^{-1}. The global annual net carbon balance was about 0.2 GtC yr^{-1}, indicating a state close to equilibrium.

Local seasonal cycles

Figs. 3 to 6 depict seasonal cycles of temperature, precipitation, plant-absorbed short-wave radiation, and soil moisture in the top graphs, growth and respiration factors in the middle graphs, and the resulting carbon fluxes NPP, total litter production, total litter decay, and net carbon flux to the atmosphere in the bottom graphs, in 4 selected regions occupied by different biomes. Since woody litter production rates were specified as being constant in time, the variations in total litter production show mainly the variations in herbaceous litter production. The same also holds essentially for the litter decay. Note the varying scales on the figures.

Tropical rain forest (Central Amazon Basin, Brazil); 1° to 3°S, 66° to 68°W

This tropical rainforest region (Fig. 3) is characterized by good growing conditions throughout the year (Fig. 3 top).

The drought index is always optimal and the temperature dependent indices, Φ_T and μ_T (Fig. 3 middle), are almost constant during the year.

Thus NPP shows only small variations, as does net carbon flux (Fig. 3 bottom). The net carbon flux is slightly positive; this results from the litter production and litter decay being slightly larger than the NPP. This imbalance is an artefact of the initialization and is unimportant on larger scales.

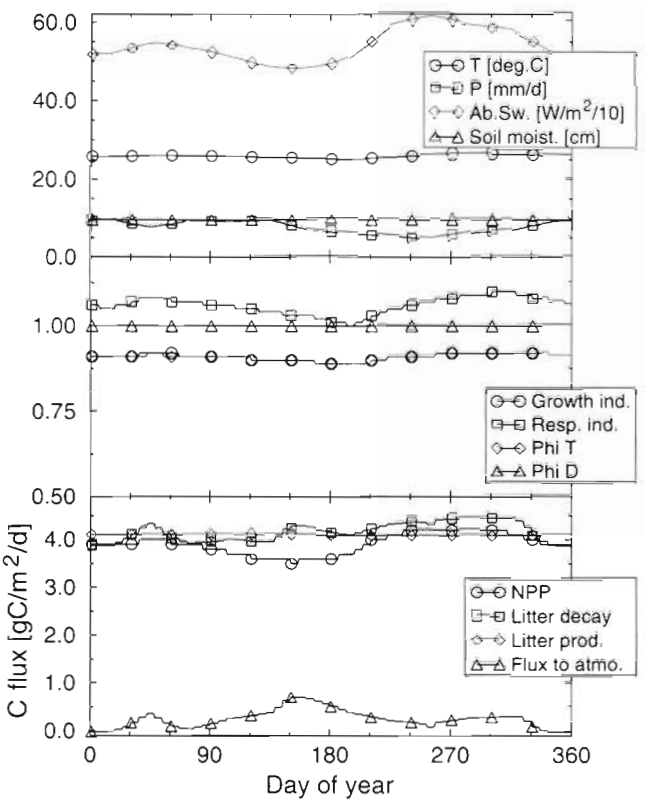

Fig. 3. Input data and model-simulated variables in a region of tropical rain forest in Central Amazon Basin, Brazil, 1° to 3° S, 66° to 68° W. Top: daily temperature, precipitation, plant-absorbed short-wave radiation, and soil moisture; middle: daily growth ($\Phi_T \times \Phi_D$) and respiration indices, and temperature and drought indices for assimilation; bottom: daily NPP, total litter production, total litter decay, and net carbon flux to the atmosphere

Tropical seasonal forest (Northern Mato Grosso, Brazil); 6° to 8°S, 56° to 58°W

In this region temperature is close to 25°C throughout the year (Fig. 4).

Precipitation shows a strong seasonality, with decreased values from mid-May to mid-September. These low precipitation values lead to a strong reduction of soil moisture and severe drought stress from July to mid-September. Despite increased sunshine, the dry season results in markedly decreased NPP values from June to September. NPP even becomes negative, due to continuously high respiration costs and reduced GPP from mid-July to the end of August. The figure also clearly shows an increase in litter production due to shedding of herbaceous biomass, resulting from the onset of the dry season. Litter decay is elevated during August to November due to the increased litter production during the dry season. These interactions add up to a positive carbon flux to the atmosphere from July to November, resulting first from decreased NPP and then from increased heterotrophic respiration. Similar soil moisture and NPP patterns were found during the FIFE field study (Desjardins et al. 1992, Verma et al. 1992).

Temperate deciduous forest (Appalachian Mountains, USA); 37° to 39°N, 76° to 78°W

At this location soil moisture shows a seasonal pattern with minimal values in summer and maximal values in winter, opposing the seasonal cycle in temperature (Fig. 5).

The seasonal development of the drought index, Φ_D, mirrors the development of soil moisture. The temperature index for assimilation, Φ_T, reaches its maximum at the end of June. Slightly decreased values during July indicate temperatures above the optimum, T_{opt}. The respiration index becomes maximal in July.

NPP increases during spring, then shows a slight summer depression and increases again in late

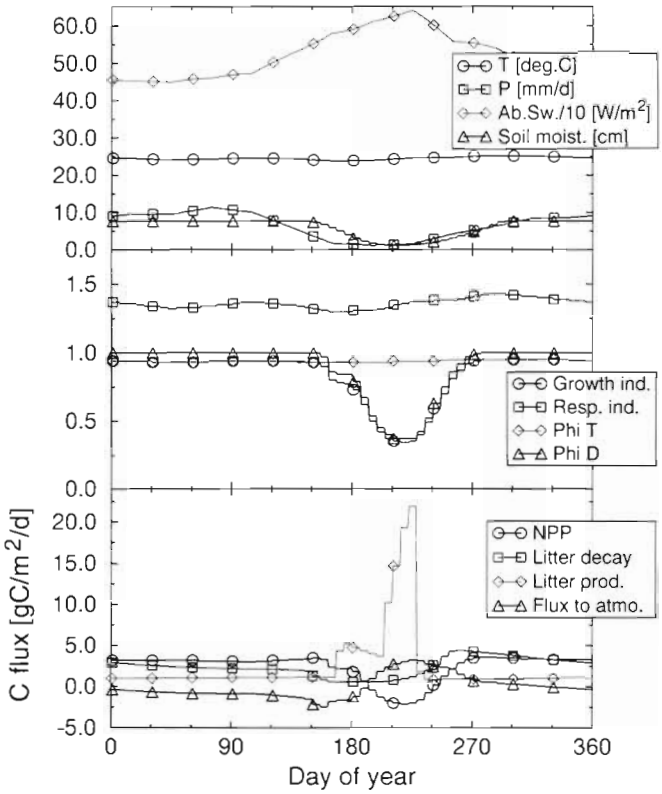

Fig. 4. Input data and model simulated variables in a region of tropical seasonal forest in Northern Mato Grosso, Brazil, 6° to 8° S, 56° to 58° W. Top: daily temperature, precipitation, plant-absorbed short-wave radiation, and soil moisture; middle: daily growth ($\Phi_T \times \Phi_D$) and respiration indices, and temperature and drought indices for assimilation; bottom: daily NPP, total litter production, total litter decay, and net carbon flux to the atmosphere

August/September. This pattern reflects the simultaneous increase of assimilation and plant respiration in spring, the depressed summer assimilation due to temperature and drought stress in June and July with further increased plant respiration, followed by decreased plant respiration but prevailing good growth conditions in August and September. Herbaceous litter production starts at the beginning of December at temperatures below 5°C. Total litter production reaches 50 gC m^{-2} d^{-1} (maximal values are not shown, for readability of the figure). The litter and SOC decay is around 2.5 gC m^{-2} d^{-1} throughout the year and rises to 5 gC m^{-2} d^{-1} during June and July. Net carbon flux to the atmosphere is positive during winter, negative for March to mid-May, then positive again due to drought stress and excessive plant respiration, and finally negative again in late summer and early autumn.

Warm grassland (Great Plains, Kansas, USA): 39° to 40° N, 99° to 101° W

This warm grassland region (Fig. 6) is characterized by low winter temperatures (below 0°C), high summer temperatures (above 25°C), and low precipitation throughout the year, with a small maximum in late spring to early summer.

These climatic conditions lead to drought stress throughout the whole year, except in winter, the drought index being below 0.5 for most of the year and 1 in winter. However, no high temperature stress on assimilation occurs despite the drought stress.

Consequently the model predicts a positive NPP throughout the whole growing season (1 to 2 gC m^{-2} d^{-1}). Leaf fall occurs at the end of winter due to the temperature-moisture relations which imply that Φ_D drops below the leaf-fall threshold of 0.4 only at this time of the year. During summer heterotrophic respiration is limited by precipitation and during winter by temperature. Throughout the summer it is higher than

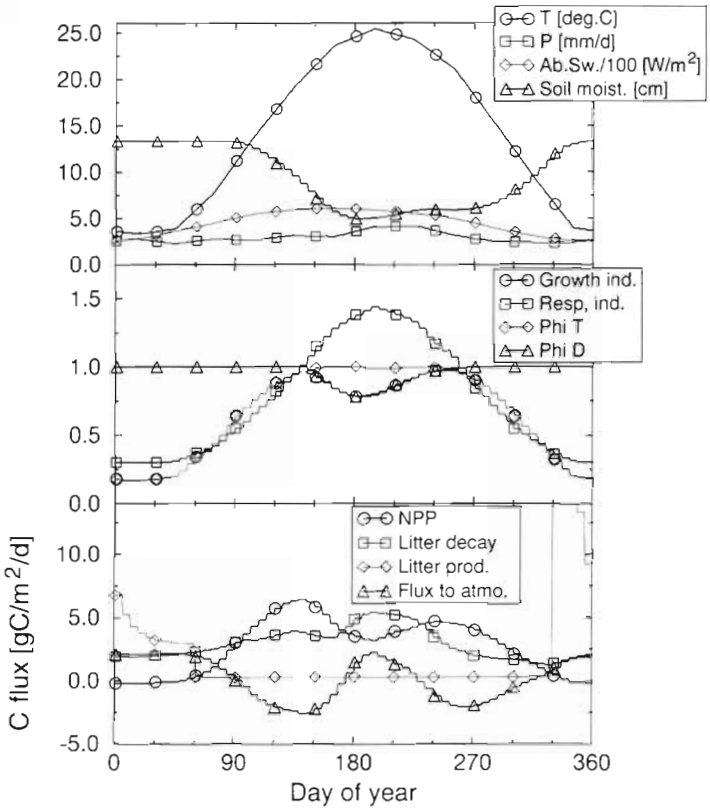

Fig. 5. Input data and model-simulated variables in a region of temperate deciduous forest in the Appalachian Mountains, USA, 37° to 39° N, 76° to 78° W. Top: daily temperature, precipitation, plant-absorbed short-wave radiation, and soil moisture; middle: daily growth ($\Phi_T \times \Phi_D$) and respiration indices, and temperature and drought indices for assimilation; bottom: NPP, total litter production, total litter decay, and net carbon flux to the atmosphere

about 1 gC m^{-2} d^{-1}; in winter and spring heterotrophic respiration remains significantly above 0, resulting in a positive carbon flux to the atmosphere during this part of the year.

Annual NPP

In order to evaluate the simulated annual NPP rates of the new model we here compare our results with (1) local ground NPP observations, (2) biome-averaged NPP from the HRBM and the data of Olson el al. (1983), and (3) the global NPP distribution predicted by the HRBM. Whenever necessary, plant dry matter units were converted to carbon units by applying a factor of 0.45 (Whittaker & Likens 1973).

Model versus ground observations: NPP

Fig. 7 shows a scatter plot comparing locally measured NPP data with the simulated annual NPP rates of the corresponding grid cells. The biome and the number of point measurements per biome are also indicated.

Such a comparison suffers intrinsically from several problems. Firstly, the model simulation represents a mean over the entire grid cell, whereas the local measurements reflect the reaction of vegetation to local conditions, which can be very different from the grid cell mean. A consequence is that the observations will exhibit more variability than the model results. Secondly, the point measurements are subject to unknown and quite often significant errors.

The observed local ground NPP rates were selected from the data of Lieth (1975) and a database of Esser (1984). We extracted from the point measurements only those points where the original description of the observed data indicated a vegetation compatible with the BIOME I classification. We thus obtained the 70 data points shown in Fig. 7.

Considering the above caveats, the figure indicates that the NPP rates of forests (Tropical Seasonal, Broadleaf Evergreen/Mixed, Temperate Deciduous, Cool Mixed, Cool Coniferous, Boreal) are in general reasonably well simulated with a tendency towards overestimation (r^2 = 0.52). The annual NPP of the Savannah points exhibits a large scatter and the model shows a general underestimation in this biome. The simulation of annual NPP rates at the points for the biomes Warm and Cool Grass/Shrub and Tundra is not satisfactory, for reasons discussed below.

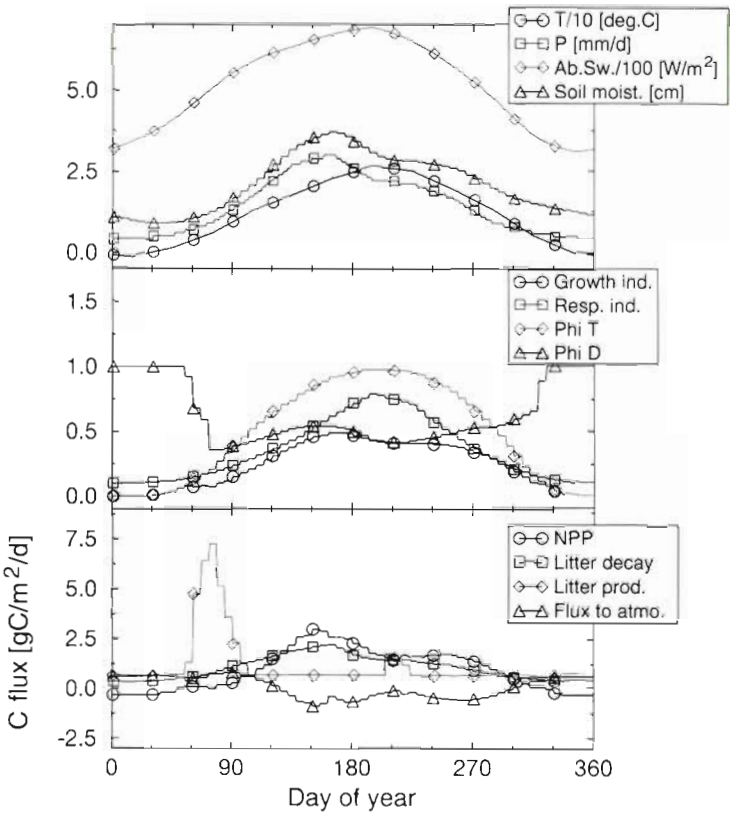

Fig. 6. Input data and model-simulated variables in a region of warm grassland in the Great Plains, Kansas, USA, 39° to 40° N, 99° to 101° W. Top: daily temperature, precipitation, plant-absorbed short-wave radiation, and soil moisture; middle: daily growth ($\Phi_T \times \Phi_D$) and respiration indices, and temperature and drought indices for assimilation; bottom: NPP, total litter production, total litter decay, and net carbon flux to the atmosphere

Model versus HRBM and Olson et al.: biome-averaged NPP

For a preliminary comparison of our model with the HRBM we used the results of a simulation experiment with the standard HRBM (Esser 1991) in which we forced the model with fixed climate using the IIASA climatologies and the observed mean annual atmospheric CO_2 concentration of 1980. From the results of the HRBM we calculated annual NPP of potential vegetation, which should be comparable with the NPP estimates of our new model. In this simulation the HRBM calculated a global potential NPP of about 51 GtC yr^{-1}. Fig. 8 shows a comparison of mean annual NPP rates simulated with the new model, with the standard HRBM, and based on observational data compiled by Olson et al. (1983).

Several caveats have to be kept in mind in such a comparison. As mentioned before, the data of Olson et al. (1983) refer to the actual natural vegetation existing

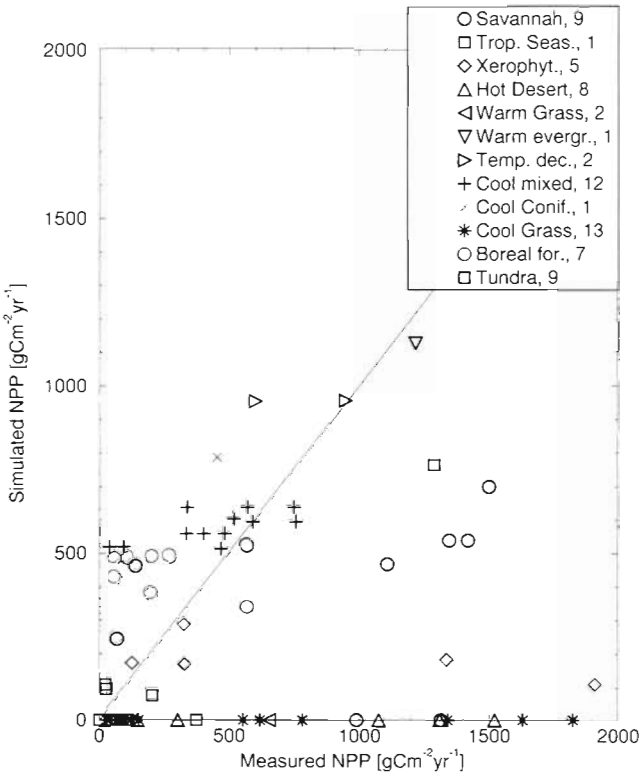

Fig. 7 Annual NPP simulated by the new model plotted against point measurements of annual NPP in different biomes. The number of point measurements in each biome is indicated

before approximately 1980, whereas both models use the BIOME I map of potential vegetation. Furthermore the vegetation classification used by Olson et al. (1983) is different from the one used in the BIOME I model. Therefore we again reassigned the Olson et al. (1983) vegetation types to corresponding BIOME I types as described previously. Finally, the compilation of Olson et al. (1983) does not contain any data on the potential natural NPP in areas subjected to anthropogenic influence (nearly all of central and eastern Europe, eastern United States, northern China, northern India, southern Australia and several other smaller regions).

On the basis of these uncertainties, Fig. 8 indicates that the new NPP model gives quite good results for most forest formations with the exception of Cold Deciduous Forest. For this biome no parameters for leaf budburst could be derived from the satellite data and therefore the same values as for Boreal Forest were used. This might be a reason for the failure of the model in this biome. The NPP estimation for Tropical Rain Forest results in values that are too high. Possibly this overestimation results from ignoring the temperature dependence of quantum yield efficiency and the fact that the model does not include growth respiration.

In addition, the results for the Grass/Shrub formations, Hot Desert, Tundra, and cool Semidesert are not satisfying. This might be related in part to the fact that the model formulation does not permit belowground biomass to be treated separately. Thus, if a large portion of the leaves are shed a corresponding proportion of fine roots is also shed as litter. Hence prerequisite for leaf growth in the next growing season is the regrowth of fine roots, as leaves and fine roots are related by a fixed root/shoot ratio. This might not be realistic in biomes dominated by herbaceous plants. In the case of hot environments the deficiencies possibly result from the fact that the model was forced with daily precipitation data obtained from a smooth distribution of precipitation throughout the month. This might lead to high drought stress throughout the whole growing period, since the soil water pool is never filled as compared to a case with few but stronger precipitation events, and we neglect any plant internal water stores.

Model versus HRBM: global NPP distribution

Figs. 9 & 10 display the global distributions of annual potential NPP simulated by the HRBM and the new model using the same climate input.

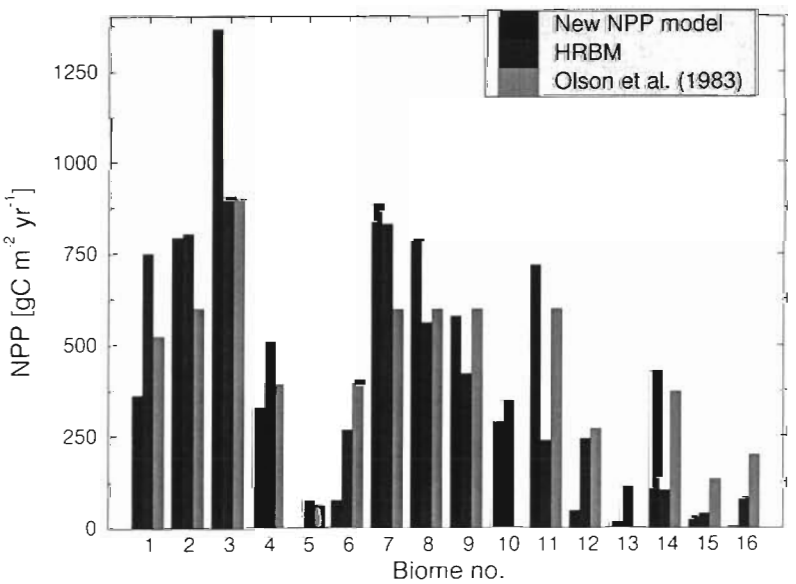

Fig. 8. Mean annual NPP for each biome from the simulations of the new model and the HRBM and from the data of Olson et al. (1983)

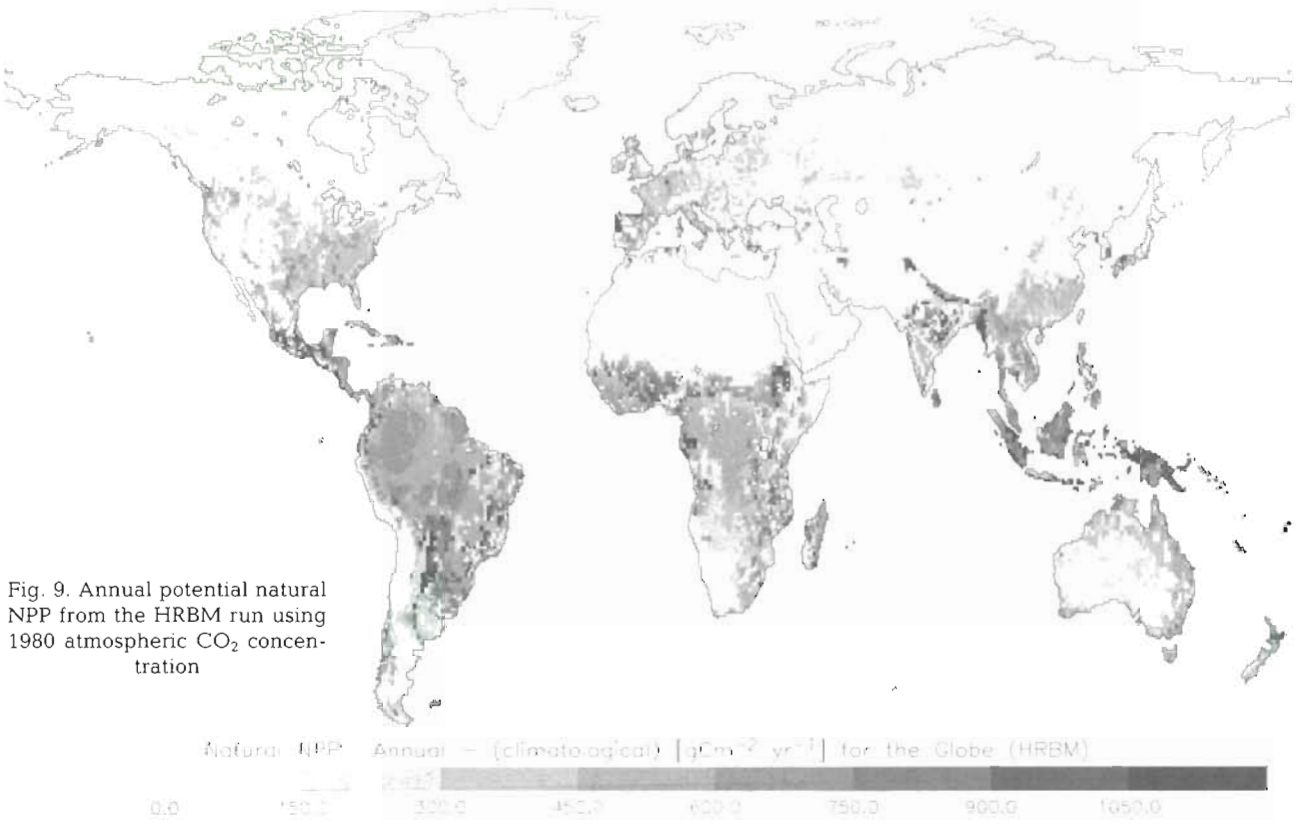

Fig. 9. Annual potential natural NPP from the HRBM run using 1980 atmospheric CO_2 concentration

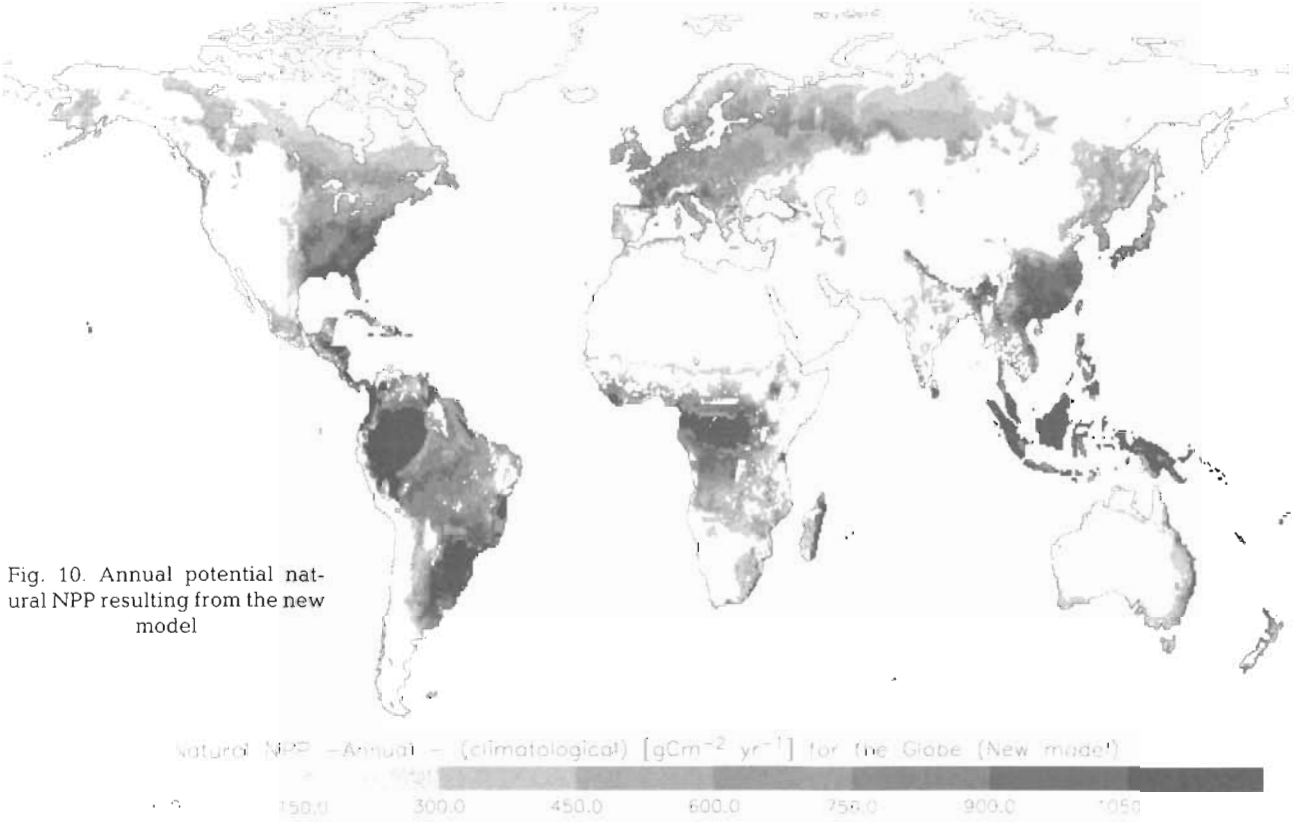

Fig. 10. Annual potential natural NPP resulting from the new model

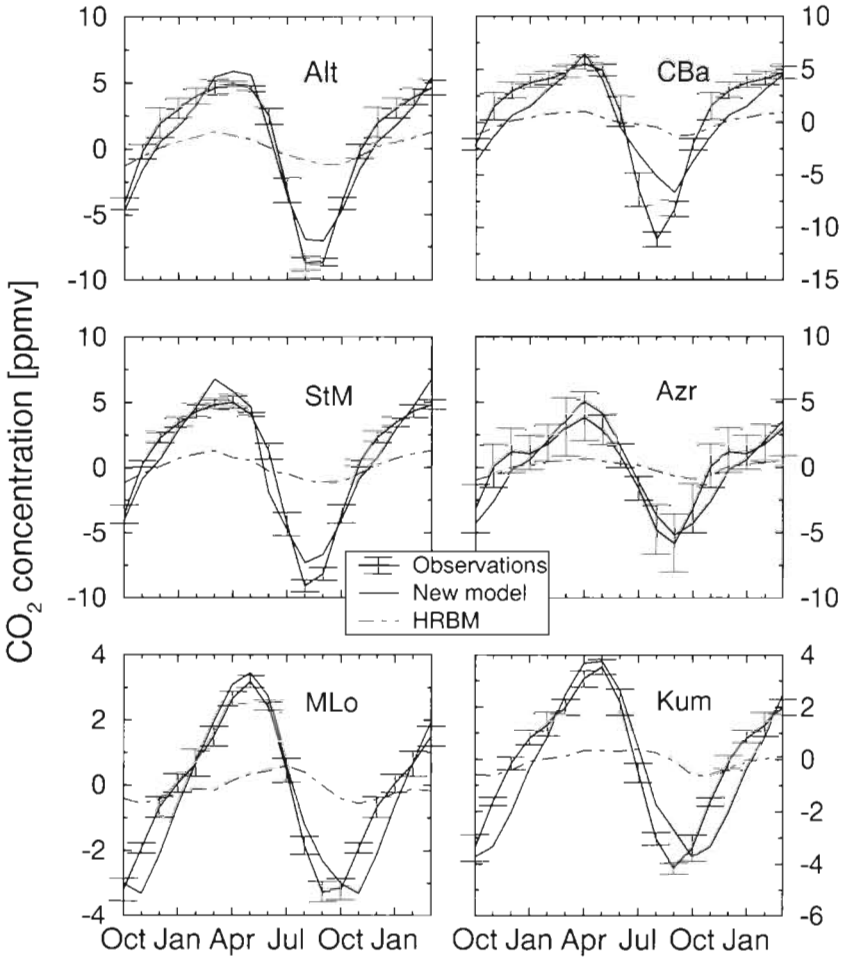

Fig. 11. Seasonal cycles of atmospheric CO_2 concentration resulting from the biospheric CO_2 fluxes of the new model (solid line) and the standard HRBM (dashed line) compared to observations (solid line with error bars indicating 1 standard deviation) at northern hemispheric stations. Alt: Alert, 82.50° N, 62.33° W; CBa: Cold Bay, 55.02° N, 162.72° W; StM: Ocean Station M, 66.00° N, 2.00° E; Azr: Azores, 38.75° N, 27.08° W; MLo: Mauna Loa, 19.53° N, 155.58° W; Kum: Cape Kumukahi, 19.52° N, 154.82° W

The weaknesses of the new model in the grass and desert biomes account for most of the areas in Fig. 10 with an annual NPP of less than 25 gC m^{-2} yr^{-1}. In the other biomes the new model generally simulates a higher annual NPP than the HRBM. Furthermore the broad features indicate that the new NPP formulation is dominated more by the biome-dependent parameters than is the HRBM formulation, which is predominantly climate- and soil-controlled.

Global net seasonal fluxes

As a final validation test we investigated the seasonal cycle of atmospheric CO_2 concentration generated by the net biospheric CO_2 fluxes of the new model, using the atmospheric transport model TM2 (Heimann & Keeling 1989, Heimann 1995). The transport model was forced with the observed winds of 1986 and was run for 4 yr to obtain a cyclo-stationary state. In the northern hemisphere the biospheric CO_2 signal dominates the annual cycles of atmospheric CO_2, whereas in the southern hemisphere oceanic exchange fluxes and seasonally varying transport processes are also important (Heimann et al. 1989). Therefore we show the results of the simulated annual cycles of atmospheric CO_2 together with observations for 6 northern hemispheric stations in Fig. 11.

The amplitude and phase of the annual cycle resulting from the new NPP model match the observations (solid line) quite well, in contrast to the annual cycle generated by the standard HRBM (dashed line) which is not pronounced enough, indicating too strong an overlap of the times of net primary production and heterotrophic respiration.

Thus our NPP and phenology modules simulate a strong drop of the atmospheric CO_2 concentration during spring in the north by allowing for a rapid budburst, which is supported by the stored assimilates.

CONCLUSIONS

New formulations for simulating the seasonal course of phenology and NPP of natural vegetation were developed and implemented as submodels in the

HRBM. The new submodels were designed as relatively independent units, facilitating their use with other terrestrial carbon cycle models. Both submodels are based on mechanistic descriptions of plant physiology and are forced with climate data.

Our initial evaluations indicate that the simulated NPP of forests is realistic. However, NPP of grass-dominated biomes is greatly underestimated and the scheme fails completely in hot desert environments.

A comparison with observed seasonal cycles of the atmospheric CO_2 concentration shows that the new model reproduces the seasonal cycle much more realistically than the standard HRBM. This indicates that the phenology scheme gives a reasonable timing of NPP versus litter decay during different times of the year, since it is the difference between these 2 CO_2 fluxes, i.e. the net flux, which is the quantity contributing to the seasonal atmospheric CO_2 variation. These results indicate that an appropriate simulation of the local seasonal cycles of CO_2 exchanges, based on climate-driven, physiologically orientated phenology schemes, seems feasible.

We limited ourselves to here to the modelling of natural vegetation, although today large parts of the vegetated land area on the earth are anthropogenically influenced. However, large fractions of the global NPP are still produced by natural or relatively undisturbed forest areas in the tropics and the boreal zone. Simulations of agricultural systems would require additional components, to account e.g. for fertilizer input or planting techniques. Conceptually our model represents a component of a more general model framework which would distinguish between natural and other vegetation types.

The new model is not yet suitable for simulations of global terrestrial carbon dynamics on interannual times scales. The NPP module must be improved to include the climate-sensitive processes of photosynthesis on a more biochemical-physiological basis, and growth respiration needs to be included. For longer simulations the soil module needs to be improved too, such that the storage and release of carbon by soils and wetlands can eventually be accounted for.

For projections into the more distant future, possibly with drastically elevated atmospheric CO_2 concentrations, the fixed ratios of woody to herbaceous biomass and aboveground to belowground biomass have to be replaced with an ecophysiologically based determination of biomass allocation. Fixed fractions are not appropriate as, for example, root/shoot ratios of many plants change under elevated CO_2 concentrations (Oechel & Strain 1985). However, it is not yet possible to conclusively assess the effects of elevated CO_2 concentration on natural ecosystems. Finally, a complete description of the terrestrial biospheric carbon cycle should include succession and migration processes. However, no such integrated description of these processes, on the landscape to continental scale, for prediction purposes is presently available. The incorporation of all these processes into a global terrestrial carbon cycle model represents a major challenge for the modelling community in the next decade.

Acknowledgements. We thank Colin Prentice for his invaluable help, in particular with the physiological part of the model; Gerd Esser for his friendly support in using the HRBM and for access to his database; Frank Mack for generously supplying the datasets on various biological parameters; Martin Claussen, Gerd Esser, Georg Hoffmann and Colin Prentice for comments on an early version of the manuscript; and 3 anonymous reviewers for their very helpful suggestions. This work was supported in part by EC projects EPOC-CT90-0017 and EV5V-CT92-0120.

LITERATURE CITED

Amthor JS (1984) The role of maintenance respiration in plant growth. Plant Cell Environ 7:561–569

Cosby BJ, Hornberger GM, Clapp RB, Ginn TR (1984) A statistical exploration of the relationships of soil moisture characteristics to the physical properties of soils. Water Resour Res 20(6):682–690

Desjardins RL, Schuepp PH, MacPherson JI, Buckley DJ (1992) Spatial and temporal variations of the fluxes of carbon dioxide and sensible and latent heat over the FIFE site. J geophys Res 97 (D7):18467–18476

Esser G (1984) The significance of biospheric carbon pools and fluxes for atmospheric CO_2: a proposed model structure. Prog Biometeorol 3:253–294

Esser G (1991) Osnabrück Biosphere Model: construction, structure, results. In: Esser G, Overdieck D (eds) Modern ecology: basic and applied aspects. Elsevier Science, Amsterdam

Esser G, Aselman I, Lieth H (1982) Modelling the carbon reservoir in the system compartment 'litter' In: Degens ET, Kempe S (eds) Transport of carbon and minerals in major world rivers, Part 1. Mitt Geol-Paläontol Inst Univ Hamburg, SCOPE/UNEP Sonderb 52:39–58

Esser G, Hoffstadt J, Mack F, Wittenberg U (1994). High Resolution Biosphere Model Version 3.00.00 — Documentation. Mitt Inst Pflanzenökol Justus-Liebig-Univ Giessen 2:1–68

Evans JR (1989) Photosynthesis and nitrogen relationships in leaves of C_3 plants. Oecologia 78:9–19

Gallo KP (1992) Experimental global vegetation index from AVHRR utilizing pre-launch calibration, cloud and sun-angle screening. Digital data. National Oceanic and Atmospheric Administration, National Geophysical Data Center, Boulder, CO

Heimann M (1995) The Global Atmospheric Tracer model TM2. Deutsches Klimarechenzentrum Tech Rep 10, Hamburg

Heimann M, Keeling CD (1989) A three-dimensional model of atmospheric CO_2 transport based on observed winds: 2. Model description and simulated tracer experiments. In: Peterson DH (ed) Aspects of climate variability in the Pacific and the Western Americas. American Geophysical Union, Washington, DC, p 165–236

Heimann M, Keeling CD, Tucker DJ (1989) A three-dimensional model of atmospheric CO_2 transport based on observed winds: 3. Seasonal cycle and synoptic time scale variations. In: Peterson DH (ed) Aspects of climate variability in the Pacific and the Western Americas. American Geophysical Union, Washington, DC, p 277–303

Janecek A, Benderoth G, Lüdeke MKB, Kindermann J, Kohlmaier GH (1989) Model of the seasonal and perennial carbon dynamics in deciduous-type forests controlled by climatic variables. Ecol Model 49:101–124

Jarvis PG, MacNaughton KG (1986) Stomatal control of transpiration: scaling up from leaf to region. Adv ecol Res 15: 1–49

Johnson FH, Eyring H, Polissar MJ (1954) The kinematic basis of molecular biology. Wiley, New York

Knorr W, Heimann M (1995) Impact of drought stress and other factors on seasonal land biosphere CO_2 exchange studied through an atmospheric tracer transport model. Tellus 47B(4):471–489

Landsberg JJ (1986) Physiological ecology of forest production. Academic Press, Orlando

Larcher W (1984) Ökologie der Pflanzen, 4th edn. Eugen Ulmer, Stuttgart

Leemans R, Cramer WP (1991) The IIASA database for mean monthly values of temperature, precipitation, and cloudiness on a global terrestrial Grid. IIASA Res Rep RR-91-18, Laxenburg, Austria

Lerch G (1991) Pflanzenökologie. Akademie Verlag, Berlin

Lieth H (1975) Modeling the primary productivity of the world. In: Lieth H, Whittaker RH (eds) Primary productivity of the biosphere. Ecological Studies 14, Springer, Berlin, p 237–264

Linacre ET (1968) Estimating the net radiation flux. Agric Meteorol 5:49–63

Lommen PW, Schwintzer CR, Yocum CS, Gates DM (1971) A model describing photosynthesis in terms of gas diffusion and enzyme kinetics. Planta 98:195–220

Lüdeke MKB, Dönges S, Otto RD, Kindermann J, Badeck, FW, Ramge P, Jäkel U, Kohlmaier GH (1995) Responses in NPP and carbon stores of the northern biomes to a CO_2-induced climatic change, as evaluated by the Frankfurt biosphere model (FBM). Tellus 47B(1/2):191–205

Mack F (1994) The influence of vegetation fires on the global carbon cycle. PhD thesis, Institute for Plant Ecology, Justus-Liebig-Universität, Giessen

Medina E, Klinge H (1983) Productivity of tropical forests and tropical woodlands. In: Lange OL et al. (eds) Physiological plant ecology IV. Springer, Berlin, p 281–303

Mitchell JFB, Manabe S, Meleshko V, Tojioka T (1990) Equilibrium climate change — and its implications for the future. In: Houghton JJ, Jenkins GJ, Ephraums JJ (eds) Climate change — the IPCC scientific assessment. Cambridge University Press, Cambridge, p 131–172

Monsi M, Saeki T (1953) Über den Lichtfaktor in Pflanzengesellschaften und seine Bedeutung für die Stoffproduktion. Jap J Bot 14:22–52

Murray MB, Cannell MGR, Smith RI (1989) Date of budburst of fifteen tree species in Britain following climate warming. J appl Ecol 26:693–700

Oechel WC, Strain BR (1985) Native species response to increased atmospheric carbon dioxide concentration. In: Strain BR, Cure JD (eds) Direct effects of increasing carbon dioxide on vegetation. DOE Rep ER-0236, US Dept of Energy, Washington, DC, p 117–154

Olson JS, Watts JA, Allison LJ (1983) Carbon in live vegetation of major world ecosystems. Report DOE/NBB-0037 for US Dept of Energy, Carbon Dioxide Research Division, Washington, DC

Prentice IC, Cramer W, Harrison SP, Monserud RA, Solomon AM (1992) A global biome model based on plant physiology and dominance, soil properties and climate. J Biogeogr 19:117–134

Prentice IC, Sykes MT, Cramer W (1993) A simulation model for the transient effects of climate change on forest landscapes. Ecol Model 65:51–70

Raich JW, Rastetter EB, Melillo JM, Kicklighter DW, Steudler PA, Peterson BJ, Grace AL, Moore III B, Vörösmarty CS (1991) Potential net primary productivity in South America: application of a global model. Ecol Appl 1(4):399–429

Ryan MG (1989) Sapwood volume for three subalpine conifers: predictive equations and ecological implications. Can J For Res 19:1397–1401

Ryan MG (1991) Effects of climate change on plant respiration. Ecol Appl 1(2):157–167

Ryan MG, Linder S, Vose JM, Hubbard RM (1993) Dark respiration in Pinaceae. Ecol Bull 43

Shinozaki K, Yoda K, Hozumi K, Kira T (1964) A quantitative analysis of plant form — the Pipe Model Theory I. Basic analyses. Jap J Ecol 14 (3):97–104

Sprugel DG, Ryan MG, Brooks JR, Vogt KA, Martin TA (1995) Respiration from the organ level to the stand. In: Smith WK, Hinckley TM (eds) Resource physiology of conifers: acquisition, allocation and utilization. Academic Press, San Diego, p 255–299

Verma SB, Kim J, Clement RJ (1992) Momentum, water vapour, and carbon dioxide exchange at a centrally located prairie site during FIFE. J geophys Res 97(D7): 18629–18640

Wardlaw IF (1990) The control of carbon partioning in plants. New Phytol 116:341–381

Waring RH, Schlesinger WH (1985) Forest ecosystems, concepts and management. Academic Press, Orlando

Webb RS, Rosenzweig CE, Levine ER (1992) A global data set of soil particle size properties. In: Global Ecosystems Database Version 1.0: Disc A, on CD-ROM. (First published 1991.) NOAA National Geophysical Data Center, Boulder, CO

Whittaker RH, Likens GE (1973) Carbon in the biota. In: Woodwell GM, Pecan EV (eds) Carbon and the biosphere. Proceedings of the 24th Brookhaven Symp Biol, Upton, New York. National Technical Information Service, Springfield, VA, p 281–302

Whittaker RH, Marks PL (1975) Methods of assessing terrestrial productivity. In: Lieth H, Whittaker RH (eds) Primary productivity of the biosphere. Ecological Studies 14, Springer, Berlin, p 55–118

Editor: H. von Storch, Hamburg, Germany

Manuscript first received: December 23, 1994
Revised version accepted: July 17, 1995

Appendix 1. Quantities used in the model: symbols, descriptions and units

State variables

pa	Content of assimilate pool; gC m^{-2}
ph	Content of living herbaceous biomass pool; gC m^{-2}
pw	Content of living woody biomass pool; gC m^{-2}
lh	Content of herbaceous litter pool; gC m^{-2}
lw	Content of woody litter pool; gC m^{-2}
soc	Content of soil organic carbon pool; gC m^{-2}
sw	Soil water; mm

Other variables

$A(z,t)$	Instantaneous gross assimilation of the leaves at height z; µmol CO_2 m^{-2} s^{-1}
B	Bole height, not explicitly required
GPP_{std}	Unstressed daily gross production; µmol CO_2 m^{-2} d^{-1}
H	Stand height, $H = 20(0.001pw^{0.521})^{0.4}$; m
$I(z,t)$	Instantaneous downward PAR at time t and height z in the canopy; µE m^{-2} s^{-1}
$I_0(t)$	Instantaneous downward non-reflected PAR at top of canopy and time t; µE m^{-2} s^{-1}
$I_{ab}(z,t)$	Instantaneous absorbed PAR at time t and height z in the canopy; µE m^{-2} s^{-1}
$L(z)$	Accumulated leaf area above height z; m^2
LAI	Leaf area index, $LAI = SLA^* \cdot ph$; m^2 m^{-2}
LAI_{max}	Maximal LAI for current timestep, $LAI_{max} = \min(LAI_{npp}, LAI_{veg})$; m^2 m^{-2}
LAI_{npp}	Point at which $\frac{dNPP}{dLAI} = 0$ in the current time step; m^2 m^{-2}
LAI_{veg}	Maximum structurally possible LAI, $LAI_{veg} = SLA^* \cdot fh \cdot p_{tot}$; m^2 m^{-2}
NPP_d	Daily NPP, $NPP_d = \Phi_T \Phi_D GPP_{std} - \mu_T R_{std}$; µmol m^{-2} s^{-1}
$P_{max}(z)$	Maximal assimilation rate of the leaves at height z, $P_{max}(z) = A_{max} e^{-ks_L(H-z)}$; µmol CO_2 m^{-2} s^{-1}
$R_l(t)$	Instantaneous outgoing long-wave radiation; W m^{-2}
$R_n(t)$	Instantaneous net radiation; W m^{-2}
$R_s(t)$	Instantaneous, non-reflected short-wave (t)radiation; W m^{-2}
R_{std}	Daily plant respiration at $T = T_{ref}$; µmol CO_2 m^{-2} d^{-1}
$Rh(z)$	Leaf plus fine root respiration rate for height z at $T = T_{ref}$, $Rh(z) = 0.1 P_{max}(z)$; µmol CO_2 m^{-2} s^{-1}
Rl_{max}	Sun leaf respiration rate at temperature $T = T_{ref}$, $Rl_{max} = 0.1 A_{max}$; µmol CO_2 m^{-2} s^{-1}
Rs	Sapwood respiration rate at temperature $T = T_{ref}$, $Rs = 100 Rl_{max}$; µmol CO_2 m^{-3} s^{-1}
$Rt(z)$	Respiration for height z at temperature $T = T_{ref}$, Eq. (20); µmol CO_2 m^{-2} s^{-1}
S	Fraction of full sunlight during daylight hours
$SAI(z)$	Sapwood cross sectional area at height z, $SAI(z) = \epsilon L(z)$; m^2 m^{-2}
SLA^*	Reduced specific leaf area, $SLA^* = \frac{t}{1+rs} SLA$; m^2 g^{-1} C
SVI	Sapwood volume index, SVI = $\epsilon LAI(z) \cdot H$; m^3 m^{-2}
T_{opt}	Optimal assimilation temperature, $T_{opt} = \frac{2}{5}(T_{min} + 1.5T_{max})$ (see Table 2); °C
T_{ref}	Reference temperature for respiration, $T_{ref} = T_{opt}$; °C
dbh	Mean diameter at breast height, $dbh = 0.001 pw^{0.521}$; m
fw	Maximal fraction of woody biomass, $fw = 1 - fh$
h_2	Fraction of assimilate pool allocated daily to herbaceous biomass
h_3	Fraction of assimilate pool allocated daily to woody biomass
ldr_x	Daily rates of heterotrophic respiration for herbaceous and woody material as well as SOC (x = h, w and s respectively)
p_{tot}	Total 'living' carbon, $p_{tot} = pa + ph + pw$; gC m^{-2}
pl_{max}	Amount of herbaceous biomass corresponding to LAI_{max}, $pl_{max} = \frac{LAI_{max}}{SLA^*}$; gC m^{-2}
s_L	Leaf density, $s_L = \frac{LAI}{H-B}$; m^2 m^{-3}
z	Independent height variable
Φ_C	CO_2 index for assimilation
Φ_D	Drought index for assimilation
Φ_T	Temperature index for assimilation
μ_T	Temperature index for plant respiration

Parameters

A_{max}	Maximal assimilation rate of sun-adapted leaves (see Table 2); µmol CO_2 m^{-2} s^{-1}
Q_∞	Solar constant, Q_∞ = 1360; W m^{-2}
SLA	Specific leaf area (see Table 2); m^2 g^{-1} C
T_{max}	Maximal assimilation temperature (see Table 2); °C
T_{min}	Minimal assimilation temperature (see Table 2); °C
a, b, c	Parameters for Eq. (26) (see Table 2)
e^*	Factor for converting µE m^{-2} s^{-1} into W m^{-2}, e^* = 0.22; MJ E^{-1}
fh	Maximal fraction of herbaceous biomass of total plant mass (see Table 2)
k	Extinction coefficient for the Beer's law formulation of light extinction in the canopy (see Table 2)
la	Mean leaf age (see Table 2); yr
lw	Mean stand age (see Table 2); yr
rs	Root/shoot ratio (see Table 2)
Γ	CO_2 compensation point, Γ = 80; ppmv
β	Plant short-wave albedo (see Table 2)
ϵ	Ratio of sapwood cross sectional area to leaf area index; m^2 m^{-2} × 10^{-4}
ϕ	Quantum yield efficiency, ϕ = 0.07; mol E^{-1}
ρ	Activation energy for respiration divided by the gas constant (see Table 2); K